A Linear Identification of Diode Models from Single I-V Characteristics of PV Panels

Li Hong Idris Lim, *Member, IEEE,* Zhen Ye, Jiaying Ye, Dazhi Yang, and Hui Du

***Abstract*—This paper presents a novel approach on diode model parameters identification from the I-V characteristics of PV panels. Other than the prevailing methodology of solving a group of nonlinear equations from a few points on the I-V curve, the proposed one views the diode model as the equivalent output of a dynamic system. From this new viewpoint, diode model parameters are linked to the transfer function (after Laplace transform) of the same dynamic system whose parameters are then identified by a simple integral-based linear square. Indoor flash test shows the accuracy and effectiveness of the proposed method, and outdoor module testing shows its ability of online monitoring and diagnostics. Comparisons to the methods of Lambert W function and evolution algorithms are also included.**

***Index Terms*—Diode model, I-V characteristics, linear least square, binary search algorithm.**

I. Introduction

THE current-voltage (I-V) characteristics of photovoltaic cell/modules play an important role in solar industry because it exactly reflects the cell/module performance [1]. Lumped-circuit models with multiple diodes (as shown in Fig.1) have been broadly accepted to accurately describe the I-V characteristics [2], where diode D_1 accounts for carriers diffusing across the P-N junction and recombining in the bulk or at surfaces. Diode D_2 is sometimes attributed to carrier recombination by traps within the depletion region [3], or recombination at an unpassivated cell edge [4]. Theoretically, more diodes ($m > 2$) can be added to the circuit in Fig.1 to better account for distributed and localized effects in solar cells like Auger recombination, but their contributions are too small as compared to D_1 and D_2 and can be negligible [5].

The general mathematical description of the diode model in Fig.1 is given by

$$\begin{aligned} I &= I_L - \sum_{i=1}^{m} I_{D_i} - I_{sh} \\ &= I_L - \sum_{i=1}^{m} I_{o_i}\left(\mathrm{e}^{\frac{V+R_sI}{a_i}} - 1\right) - \frac{V+R_sI}{R_{sh}}, \end{aligned} \tag{1}$$

Manuscript received August 3, 2014; revised October 29, 2014 and November 28, 2014; accepted December 16, 2014.

Li Hong Idris Lim is with Department of Electronic Systems, University of Glasgow, Glasgow G12 8QQ, United Kingdom (corresponding author to provide e-mail: LiHonIdris.Lim@glasgow.ac.uk).

Zhen Ye is with REC Cells Pte Ltd., 20 Tuas South Avenue 14, Singapore 637312.

Jiaying Ye, Dazhi Yang and Hui Du are with Solar Energy Research Institute of Singapore (SERIS), National University of Singapore (NUS), Singapore 117574.

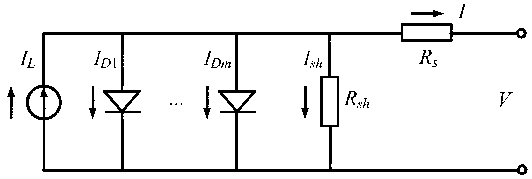

Fig. 1. Equivalent circuit of diode models

where I_L is the photocurrent proportional to the irradiance; I_{o_i} is the reverse saturation, $a_i = N_s n_i k T_c/q$ is the modified ideality factor [6] for the ith diode (N_s is the number of cells connected in series, n_i is the ideality factor, k is Boltzmann's constant, T_c is the cell temperature, and q is the electronic charge); R_s and R_{sh} are resistances in series and parallel, respectively. Only I and V are known variables from the data sheet or real measurements.

Due to the inherent nonlinearity, it is not straightforward to determine the model parameters (I_L, I_o, a, R_s and R_{sh}) from the input-output data (I-V characteristics), even for the simplest case of $m = 1$. The current methods in literature can be divided into two categories.

One category is the deterministic solution, which solves the five model parameters ($m = 1$) from the five independent equations. Usually, the four independent equations are chosen from the open-circuit, short-circuit and maximum power points at STC (1000 W/m^2, $T_c = 25$°C, AM $= 1.5$) as follows.

At short circuit (SC, $V = 0$):

$$I_{sc} = I_L - I_o\left(\mathrm{e}^{\frac{R_sI_{sc}}{a}} - 1\right) - \frac{R_sI_{sc}}{R_{sh}}. \tag{2}$$

At open circuit (OC, $I = 0$):

$$I_L - I_o\left(\mathrm{e}^{\frac{V_{oc}}{a}} - 1\right) - \frac{V_{oc}}{R_{sh}} = 0. \tag{3}$$

At maximum power point (MPP):

$$I_{mpp} = I_L - I_o\left(\mathrm{e}^{\frac{V_{mpp}+R_sI_{mpp}}{a}} - 1\right) - \frac{V_{mpp}+R_sI_{mpp}}{R_{sh}}. \tag{4}$$

$$\left.\frac{\mathrm{d}IV}{\mathrm{d}V}\right|_{mpp} = -\frac{V_{mpp}}{R_s + \frac{1}{\frac{I_o}{a}\mathrm{e}^{\frac{V_{mpp}+I_{mpp}R_s}{a}} + \frac{1}{R_{sh}}}} + I_{mpp} = 0. \tag{5}$$

There are many options for the 5th independent equation: One way is to estimate one of the five parameters independently. For example, I_L can be estimated from the influence of the structure parameters of a silicon solar cell on photocurrent [7]. I_o is material independent and can be explicitly related to a solid state parameter, the $0K$ Debye temperature of

the semiconductor [8]. a can be determined from the use of properties of special trans function theory (STFT) [9]. R_{sh} can be approximated by the inverse of the slope at SC [10], i.e., $\mathrm{d}I/\mathrm{d}V|_{sc} \approx -1/R_{sh}$. R_s estimation are well summarised in [11]–[14]. The other way is to apply one of (2)-(5) to non-STC. For example, applying (3) to $T_c^* = T_c + \Delta T$ ($\Delta T \neq 0$) gives [15]

$$0 = I_L + \alpha_T \Delta T - I_o \left(\frac{T_c^*}{T_c}\right)^3 \mathrm{e}^{\frac{E_g}{kT_c} - \frac{E_g(1-0.0002677\Delta T)}{kT_c^*}} \times \left(\mathrm{e}^{\frac{V_{oc}+\beta_T\Delta T}{a}\frac{T_c}{T_c^*}} - 1\right) - \frac{V_{oc}+\beta_T\Delta T}{R_{sh}},$$

where $E_g = 1.17 - 4.73 \times 10^{-4} T_c^2/(T_c + 636)$ is the band gap energy; α_T and β_T are the temperature coefficient of SC current and OC voltage, respectively.

No matter what the 5th equation is, if the approximated parameter is significantly different from the real value, it may lead to a singular solution to the rest of four parameters [16]. Even if there is no approximation in the 5th equation, there are no analytical solutions available due to the inherent nonlinearity. Usually, partial linearization has to be made to yield empirical formulas [17]–[21], which is a trade-off between simplicity and accuracy.

The other category is the optimal solution, which employs nonlinear fitting procedures based on the minimisation of deviations between modelled and measured I-V curves, in accordance with some metric function (usually least square) [22]–[25]. Iterative searching algorithms are usually used [26], [27], but their convergence and accuracy heavily depend on the initial values and are easily trapped in the local optimums. For different initial value guess, such approaches can result in widely different parameter sets, all leading to satisfactory curve fitting [28]. Although a good match between estimation and measured data can be obtained, there is no guarantee that the estimated I-V curve would pass the SC, OC and MPP points. To achieve the global optimum, evolution algorithms like differential evolution (DE) and genetic algorithm (GA) have to be used [29], [30]. But they are too complicated to be implemented as online calculation.

The current trend is to combine the above two categories, i.e., employing both nonlinear fitting procedure and algebraic equations solving [31]–[33]. With a single parameter fitting procedure, numerical solutions to (2)-(5) will be obtained by empirical formulas or iterative algorithms. The drawbacks of the above two categories are mitigated in this way. Recent progress is reported by Laudani *et al.* [15], [34]. By applying the Lambert W function [35], [36] to (1) ($m = 1$), the implicit format of I is converted to its equivalent explicit format as

$$I = \frac{R_{sh}(I_L + I_o) - V}{R_s + R_{sh}} - \frac{a}{R_s} W\left(\frac{I_o R_s R_{sh}}{a(R_s + R_{sh})} \mathrm{e}^{\frac{R_{sh}(V + R_s(I_L + I_o))}{a(R_s + R_{sh})}}\right). \quad (6)$$

The benefit of (6) over (1) is that the former is not transcendental anymore, which makes it possible to find solutions to (2)-(5) by iterative algorithms. Laudani *et al.* further reduce the dimension of searching space from 5 to 2 by splitting the model parameters into two independent unknowns (a and R_s) and three dependent ones (I_L, I_o and R_{sh}). In this way, the burden of iterative searching is greatly relieved and it becomes easy to get a and R_s numerically or graphically. To the best of our knowledge, this represents the best achievement ever reported in the literature.

This paper opens a new angle to view the diode model from the systems perspective. Actually, one of the biggest application of Lambert W function is to solve differential equations, which is directly linked to the representation of a linear system in time domain. For example, the first-order linear system can be described as $T\mathrm{d}y(t)/\mathrm{d}t + y(t) = u(t)$, whose unit ramp response, $y(t) = t + T(\mathrm{e}^{-t/T} - 1)$, has the same format as (1). This motivates us that the I-V curve governed by (1) can be viewed as the output of some linear system, and the model parameters can be linked to the parameters of a linear differential equation, which is then determined by system identification methods available in the literature [37], where linear least squares is good enough to yield satisfactory solutions.

The whole paper is organised as follows. Section II describes the way to transform the static I-V curve to the dynamic linear system output. Integral-based system identification methods and linear least square algorithm are then proposed in Section III. Examples of indoor flash test and applications of outdoor module testing are given in Section IV to illustrate the accuracy and effectiveness of the proposed method. Comparison with the existing methods is demonstrated in Section V. Section VI draws the conclusion.

II. Dynamic system formulation

A. One-diode model

Recall I-V curve described by (1) with $m = 1$. Let $y = I$ and $x = V + R_s I$, (1) then becomes

$$y = I_L + I_o - I_o \mathrm{e}^{\frac{x}{a}} - \frac{x}{R_{sh}}. \quad (7)$$

Taking differential once on both sides of (7) gives

$$\frac{\mathrm{d}y}{\mathrm{d}x} = -\frac{I_o}{a}\mathrm{e}^{\frac{x}{a}} - \frac{1}{R_{sh}}. \quad (8)$$

Differentiating once more for (8) gives

$$\frac{\mathrm{d}^2 y}{\mathrm{d}x^2} = -\frac{I_o}{a^2}\mathrm{e}^{\frac{x}{a}}. \quad (9)$$

Eliminating $\mathrm{e}^{x/a}$ from (8) and (9) gives

$$a\frac{\mathrm{d}^2 y}{\mathrm{d}x^2} - \frac{\mathrm{d}y}{\mathrm{d}x} = \frac{1}{R_{sh}}. \quad (10)$$

Let $t = x$ and $u(t) \equiv 1$, (10) is equivalent to

$$a\frac{\mathrm{d}^2 y(t)}{\mathrm{d}t^2} - \frac{\mathrm{d}y(t)}{\mathrm{d}t} = \frac{u(t)}{R_{sh}}, \quad (11)$$

which is a standard differential equation representation of a second order linear system. t is the "time", $u(t)$ and $y(t)$ are the system "input" and "output", respectively. Since $u(t) \equiv 1$, $y(t)$ is the unit step response of the system in "time" domain.

Take Laplace transform, $F(s) = \mathcal{L}[f(t)] = \int_0^\infty \mathrm{e}^{-st} f(t)\mathrm{d}t$, on both sides of (11),

$$a[s^2Y(s) - sy(0) - y'(0)] - [sY(s) - y(0)] = \frac{U(s)}{R_{sh}}. \quad (12)$$

Utilize $sU(s) = 1$, and (12) is equivalent to

$$a\left[s^2Y(s) - s^2U(s)y(0) - sU(s)y'(0)\right] - [sY(s) - sU(s)y(0)] = \frac{1}{R_{sh}}U(s).$$

It follows from (7) that $y(0) = I_L$, $y'(0) = -I_o/a - 1/R_{sh}$, so the transfer function from $Y(s)$ to $U(s)$ is

$$G(s) := \frac{Y(s)}{U(s)} = \frac{ay(0)s^2 + [ay'(0) - y(0)]s + \frac{1}{R_{sh}}}{as^2 - s} = \frac{aI_Ls^2 - (I_o + \frac{a}{R_{sh}} + I_L)s + \frac{1}{R_{sh}}}{as^2 - s}. \quad (13)$$

The corresponding time domain differential equation is

$$a\frac{\mathrm{d}^2y(t)}{\mathrm{d}t^2} - \frac{\mathrm{d}y(t)}{\mathrm{d}t} = aI_L\frac{\mathrm{d}^2u(t)}{\mathrm{d}t^2} - \left(I_L + I_o + \frac{a}{R_{sh}}\right) \times \frac{\mathrm{d}u(t)}{\mathrm{d}t} + \frac{u(t)}{R_{sh}}. \quad (14)$$

It should be noted that (11) is different from (14) because of the non-zero initial conditions. In other words, (14) is the description of the same system of (11) but with zero initial conditions. This will facilitate the calculation of the integral-based identification proposed in Section III.

B. Multi-diode model

Similarly by letting $y = I$ and $x = V + R_sI$ in (1), it yields

$$y = I_L + \sum_{i=1}^m I_{o_i} - \sum_{i=1}^m I_{o_i}\mathrm{e}^{\frac{x}{a_i}} - \frac{x}{R_{sh}}. \quad (15)$$

Taking differential once on both sides of (15) gives

$$\frac{\mathrm{d}y}{\mathrm{d}x} = -\sum_{i=1}^m \frac{I_{o_i}}{a_i}\mathrm{e}^{\frac{x}{a_i}} - \frac{1}{R_{sh}}. \quad (16)$$

Differentiating (16) for k times, $k = 1, 2, \cdots, m$, yields

$$y^{(k+1)}(x) = -\sum_{i=1}^m \frac{I_{o_i}}{a_i^{k+1}}\mathrm{e}^{\frac{x}{a_i}}, \quad (17)$$

where $y^{(k)}(x) = \mathrm{d}^k y/\mathrm{d}x^k$. Rewrite (17) in matrix format,

$$\underbrace{\begin{bmatrix} y^{(2)}(x) \\ y^{(3)}(x) \\ \vdots \\ y^{(m+1)}(x) \end{bmatrix}}_{B} = \underbrace{\begin{bmatrix} a_1^{-1} & a_2^{-1} & \cdots & a_m^{-1} \\ a_1^{-2} & a_2^{-2} & \cdots & a_m^{-2} \\ \vdots & \vdots & \ddots & \vdots \\ a_1^{-m} & a_2^{-m} & \cdots & a_m^{-m} \end{bmatrix}}_{A} \begin{bmatrix} -\frac{I_{o_1}}{a_1}\mathrm{e}^{\frac{x}{a_1}} \\ -\frac{I_{o_2}}{a_2}\mathrm{e}^{\frac{x}{a_2}} \\ \vdots \\ -\frac{I_{o_m}}{a_m}\mathrm{e}^{\frac{x}{a_m}} \end{bmatrix}.$$

Since $a_k \neq 0$, A is a Vandermonde matrix with $\det(A) \neq 0$, so A^{-1} exists and

$$\left[-\frac{I_{o_1}}{a_1}\mathrm{e}^{\frac{x}{a_1}}, -\frac{I_{o_2}}{a_2}\mathrm{e}^{\frac{x}{a_2}}, \ldots - \frac{I_{o_m}}{a_m}\mathrm{e}^{\frac{x}{a_m}}\right]^T = A^{-1}B, \quad (18)$$

where $A^{-1} = [\xi_{i,j}] \in \mathbb{R}_{m\times m}$ with

$$\xi_{i,j} = \frac{\sum_{\substack{1\le k_1<\cdots<k_{n-j}\le n \\ k_1,\cdots,k_{n-j}\neq i}} (-1)^{j-1}a_{k_1}^{-1}\cdots a_{k_{n-j}}^{-1}}{a_i^{-1}\prod_{\substack{1\le k\le n \\ k\neq i}}\left(a_k^{-1} - a_i^{-1}\right)}. \quad (19)$$

Substituting (18) into (16) yields

$$y^{(1)}(x) - \sum_{j=1}^m\sum_{i=1}^m \xi_{i,j}y^{(j+1)}(x) = -\frac{1}{R_{sh}}. \quad (20)$$

Let $t = x$ and $u(t) \equiv 1$, (20) becomes the differential equation representation of an mth-order "dynamic" system:

$$y^{(1)}(t) - \sum_{j=1}^m\sum_{i=1}^m \xi_{i,j}y^{(j+1)}(t) = -\frac{u(t)}{R_{sh}}. \quad (21)$$

Taking Laplace transform for both sides of (21) yields

$$sY(s) - y(0) - \sum_{j=1}^m\sum_{i=1}^m \xi_{i,j}\left(s^{j+1}Y(s) - \sum_{k=1}^{j+1} s^{k-1}y^{(j+1-k)}(0)\right) = -\frac{U(s)}{R_{sh}}. \quad (22)$$

It follows from (15)-(17) that $y(0) = I_L$, $y^{(1)}(0) = -\sum_{i=1}^m I_{o_i}/a_i - 1/R_{sh}$, $y^{(k+1)}(0) = -\sum_{i=1}^m I_{o_i}/a_i^{k+1}$ for $k = 1, 2, \cdots, m$. Since $sU(s) = 1$, (22) becomes

$$sY(s) - I_LsU(s) - \sum_{j=1}^m\sum_{i=1}^m \xi_{i,j}\left[s^{j+1}Y(s) - U(s)\times \left(\sum_{k=1}^j s^k\sum_{i=1}^m \frac{-I_{o_i}}{a_i^{j+1-k}} - \frac{s^j}{R_{sh}} + I_Ls^{j+1}\right)\right] = -\frac{U(s)}{R_{sh}}.$$

The transfer function is $G(s) = Y(s)/U(s) = N/D$, where

$$D = \sum_{j=1}^m\sum_{i=1}^m \xi_{i,j}s^{j+1} - s,$$

$$N = \frac{1}{R_{sh}} - I_Ls + \sum_{j=1}^m\sum_{i=1}^m \xi_{i,j}\times \left(I_Ls^{j+1} - \frac{s^j}{R_{sh}} - \sum_{k=1}^j s^k\sum_{i=1}^m \frac{I_{o_i}}{a_i^{j+1-k}}\right).$$

The corresponding time domain differential equation with zero initial condition is

$$\alpha_{m+1}y^{(m+1)}(t) + \cdots + \alpha_2y^{(2)}(t) - y^{(1)}(t) = \beta_{m+1}u^{(m+1)}(t) + \cdots + \beta_1u^{(1)}(t) + \frac{u(t)}{R_{sh}}, \quad (23)$$

where for $j = 1, 2, \cdots, m$,

$$\alpha_{j+1} = \sum_{i=1}^m \xi_{i,j}, \quad (24)$$

$$\beta_{m+1} = \alpha_{m+1}I_L, \quad (25)$$

$$\beta_j = \alpha_jI_L - \frac{\alpha_{j+1}}{R_{sh}} - \sum_{k=j}^m\sum_{i=1}^m \frac{\alpha_{k+1}I_{o_i}}{a_i^{k+1-j}}, \quad (26)$$

$$(\alpha_1 = -1).$$

In general, by introducing a virtual "time" of $t = x$, the static relationship between two variables y and x can be regarded as dynamics from the linear system governed by (23). Once α_i and β_i are determined from system identification, diode model parameters I_L, I_{o_i}, a_i and R_{sh} can be solved linearly from (24)-(26).

III. Integral-based linear identification

For an integer $n \geq 1$, define the multiple integral as [37]

$$\int_{[T_1,T_2]}^{(n)} f(\tau) = \underbrace{\int_{T_1}^{T_2}\int_{T_1}^{\tau_n}\cdots\int_{T_1}^{\tau_2}}_{n} f(\tau_1)\mathrm{d}\tau_1\mathrm{d}\tau_2\cdots\mathrm{d}\tau_n. \quad (27)$$

A. One-diode model

Applying (27) to (14) for $T_1 = 0$, $T_2 = t$ and $n = 2$ gives

$$ay(t) - aI_L u(t) + \left(I_L + I_o + \frac{a}{R_{sh}}\right)\int_{[0,t]}^{(1)} u(\tau) - \frac{1}{R_{sh}}\int_{[0,t]}^{(2)} u(\tau) = \int_{[0,t]}^{(1)} y(\tau). \quad (28)$$

Let $\gamma(t) = \int_{[0,t]}^{(1)} y(\tau)$, $\theta = \left[a, aI_L, \left(I_L + I_o + \frac{a}{R_{sh}}\right), \frac{1}{R_{sh}}\right]^T$, $\phi(t) = \left[y(t), -u(t), \int_{[0,t]}^{(1)} u(\tau), -\int_{[0,t]}^{(2)} u(\tau)\right]^T$, and (28) can be rewritten as the matrix format of $\phi^T(t)\theta = \gamma(t)$. Note that the matrix format holds for any $t_i \in [0,t]$, $i = 1, 2, \cdots, N$, where N is the the number of data samples on the I-V curve. This actually casts an equation group of $\Phi\theta = \Gamma$ with $\Phi = [\phi(t_1), \phi(t_2), \cdots, \phi(t_N)]^T$ and $\Gamma = [\gamma(t_1), \gamma(t_2), \cdots, \gamma(t_N)]^T$. If $\Phi^T\Phi$ is nonsingular, the linear least square solution for θ is given by

$$\theta = \left(\Phi^T\Phi\right)^{-1}\Phi^T\Gamma, \quad (29)$$

which will minimise the square error of $(\Gamma - \Phi\theta)^T(\Gamma - \Phi\theta)$. Once θ is determined from (29), the parameters of one-diode model can be obtained by $a = \theta_1$, $I_L = \theta_2/\theta_1$, $I_o = \theta_3 - \theta_2/\theta_1 - \theta_1\theta_4$, $R_{sh} = 1/\theta_4$.

B. Multi-diode model

Apply (27) to (23) for $T_1 = 0$, $T_2 = t$ and $n = m + 1$,

$$\alpha_{m+1}y(t) + \cdots + \alpha_2\int_{[0,t]}^{(m-1)} y(\tau) - \int_{[0,t]}^{(m)} y(\tau) = \beta_{m+1}u(t) + \cdots + \beta_1\int_{[0,t]}^{(m)} u(\tau) + \frac{1}{R_{sh}}\int_{[0,t]}^{(m+1)} u(\tau).$$

Let $\gamma(t) = \int_{[0,t]}^{(m)} y(\tau)$, $\theta = [\alpha_{m+1}, \cdots, \alpha_2, \beta_{m+1}, \cdots, \beta_1, 1/R_{sh}]^T$, $\phi(t)$=$[y(t), \cdots, \int_{[o,t]}^{(m-1)} y(\tau), -u(t), \cdots, -\int_{[0,t]}^{(m+1)} u(\tau)]^T$, θ and $\phi(t) \in \mathbb{R}_{(2m+2)\times 1}$, we have $\phi^T(t)\theta = \gamma(t)$. For $t_i \in [0,t]$, $i = 1, 2, \cdots, N$, the equation group can be described by $\Phi\theta = \Gamma$ with $\Phi = [\phi(t_1), \phi(t_2), \cdots, \phi(t_N)]^T$ and $\Gamma = [\gamma(t_1), \gamma(t_2), \cdots, \gamma(t_N)]^T$. If $\Phi^T\Phi$ is nonsingular, the least square solution for θ will be

$$\theta = \left(\Phi^T\Phi\right)^{-1}\Phi^T\Gamma. \quad (30)$$

Once θ is determined from (30), $R_{sh} = 1/\theta_{2m+2}$ is immediately derived. It follows from (25) that $I_L = \beta_{m+1}/\alpha_{m+1} = \theta_{m+1}/\theta_1$. a_i, $i = 1, 2, \cdots, m$, will be derived in the following way. Rewriting (24) in matrix format gives

$$[\alpha_2, \cdots, \alpha_{m+1}] = \underbrace{[1, \cdots, 1]}_{m} A^{-1}.$$

Right-multiplying A for both sides gives

$$[\alpha_2, \cdots, \alpha_{m+1}]\begin{bmatrix} a_1^{-1} & \cdots & a_m^{-1} \\ \vdots & \ddots & \vdots \\ a_1^{-m} & \cdots & a_m^{-m} \end{bmatrix} = \underbrace{[1, \cdots, 1]}_{m},$$

which implies that $1/a_i$, $(i = 1, 2, \cdots, m)$ are the roots of the following characteristic equation

$$\alpha_{m+1}\lambda^m + \alpha_m\lambda^{m-1} + \cdots + \alpha_2\lambda - 1 = 0. \quad (31)$$

Solve (31) for λ_i, and $a_i = 1/\lambda_i$, $(i = 1, 2, \cdots, m)$. I_{o_i}, $i = 1, 2, \cdots, m$, will be derived as follows. (26) can be rewritten as

$$\beta_j = \alpha_j I_L - \frac{\alpha_{j+1}}{R_{sh}} - \sum_{i=1}^{m} I_{o_i}\sum_{k=j}^{m}\frac{\alpha_{k+1}}{a_i^{k+1-j}}.$$

Rewrite further as matrix format,

$$\underbrace{\begin{bmatrix} \sum_{k=1}^{m}\frac{\alpha_{k+1}}{a_1^k} & \sum_{k=1}^{m}\frac{\alpha_{k+1}}{a_2^k} & \cdots & \sum_{k=1}^{m}\frac{\alpha_{k+1}}{a_m^k} \\ \sum_{k=2}^{m}\frac{\alpha_{k+1}}{a_1^{k-1}} & \sum_{k=2}^{m}\frac{\alpha_{k+1}}{a_2^{k-1}} & \cdots & \sum_{k=2}^{m}\frac{\alpha_{k+1}}{a_m^{k-1}} \\ \vdots & \vdots & \ddots & \vdots \\ \sum_{k=m}^{m}\frac{\alpha_{k+1}}{a_1^{k+1-m}} & \sum_{k=m}^{m}\frac{\alpha_{k+1}}{a_2^{k+1-m}} & \cdots & \sum_{k=m}^{m}\frac{\alpha_{k+1}}{a_m^{k+1-m}} \end{bmatrix}}_{\Psi} \times \begin{bmatrix} I_{o_1} \\ I_{o_2} \\ \vdots \\ I_{o_m} \end{bmatrix} = -\underbrace{\begin{bmatrix} \beta_1 + I_L + \frac{\alpha_2}{R_{sh}} \\ \beta_2 - \alpha_2 I_L + \frac{\alpha_3}{R_{sh}} \\ \vdots \\ \beta_m - \alpha_m I_L + \frac{\alpha_{m+1}}{R_{sh}} \end{bmatrix}}_{\Xi}$$

Note from (31) that $\sum_{k=1}^{m}\alpha_{k+1}/a_i^k = 1$ for $i = 1, 2, \cdots, m$, Ψ can be simplified as

$$\Psi = \underbrace{\begin{bmatrix} 1 & 1 & \cdots & 1 \\ a_1 & a_2 & \cdots & a_m \\ \vdots & \vdots & \ddots & \vdots \\ a_1^{m-1} & a_2^{m-1} & \cdots & a_m^{m-1} \end{bmatrix}}_{\Psi^*} - \begin{bmatrix} 0 & \cdots & 0 \\ \alpha_2 & \cdots & \alpha_2 \\ \vdots & \ddots & \vdots \\ \sum_{k=1}^{m-1}\alpha_{k+1}a_1^{m-1-k} & \cdots & \sum_{k=1}^{m-1}\alpha_{k+1}a_m^{m-1-k} \end{bmatrix}.$$

This implies that after elementary row operations, Ψ is similar to Ψ^*, which is a Vandermonde matrix with $\det(\Psi^*) \neq 0$. Therefore, Ψ^{-1} exists (Ψ is full rank) and $[I_{o_1}, I_{o_2}, \cdots, I_{o_m}]^T = \Psi^{-1}\Xi$.

C. Nonsingularity of $\Phi^T\Phi$

The existence of the linear least square solution by (29) and (30) depends on the nonsingularity of $\Phi^T\Phi$, which is shown by the following lemma.

Lemma 1: $\Phi^T\Phi$ is nonsingular if $a_i \neq a_j$ for $i \neq j$, $i, j = 1, 2, \cdots, m$, and the sampling number $N \geq 2m + 2$.

Proof: See Appendix. ∎

D. Calculation of multiple integrals

In practice, the integral shown as (27) is numerically estimated by rectangular or trapezoidal integration. For example, suppose there are N samples at $t_1, t_2, \cdots, t_N$, the rectangular integration gives

$$\begin{aligned}
&\int_{[t_1,t_i]}^{(1)} f(\tau) = \int_{t_1}^{t_i} f(\tau_1)\mathrm{d}\tau_1 \approx \sum_{k=1}^{i-1} f(k)(t_{k+1} - t_k) := f_1(i),\\
&\int_{[t_1,t_i]}^{(2)} f(\tau) \approx \sum_{k=1}^{i-1} f_1(k)(t_{k+1} - t_k) := f_2(i),\\
&\qquad\vdots\\
&\int_{[t_1,t_i]}^{(n)} f(\tau) \approx \sum_{k=1}^{i-1} f_{n-1}(k)(t_{k+1} - t_k) := f_n(i).
\end{aligned}$$

for $i = 1, 2, \cdots, N$. The more number of samples, f_i, the more accurate the estimation to the multiple integrals will be.

E. Determination of R_s

To calculate θ from (29) or (30), Φ and Γ must be known. As both of them are integrals to t, t must be known as well. Since $t = V + R_sI$, R_s must be determined before applying integrals. It is clear to see that if R_s is bigger than its real value, t will increase so that the whole I-V curve will move to the right and the error between the real and estimated I-V curves will be positive; If R_s decreases, the whole I-V curve will move to the left and the error between the real and estimated I-V curves will be negative. Thus, R_s can be used as a tuning parameter such that the root mean square error (RMSE) is minimised.

It derives from (1) that

$$-\frac{1}{\frac{\mathrm{d}I}{\mathrm{d}V}\big|_{oc}} = R_s + \frac{1}{\sum\limits_{i=1}^{m} \frac{I_{o_i}}{a_i}\mathrm{e}^{\frac{V_{oc}}{a_i}} + \frac{1}{R_{sh}}} > R_s,$$

which implies the upper bound of R_s, i.e., $R_s^{upp} = -1/\left.\frac{\mathrm{d}I}{\mathrm{d}V}\right|_{oc}$. The lower bound of R_s can be zero at first, i.e., $R_s^{low} = 0$. With such a band of $R_s \in [R_s^{low}, R_s^{upp}]$, binary search algorithm is applied to determine R_s in the following way:

Step 1: Arbitrarily choose R_s from $[R_s^{low}, R_s^{upp}]$ and calculate $\hat{a}_i$, $\hat{I}_L$, $\hat{I}_{o_i}$ and $\hat{R}_{sh}$ from the proposed linear least square (29) or (30);

Step 2: Calculate from (1) that

$$\hat{y}(t) = \hat{I}_L - \sum_{i=1}^{m} \hat{I}_{o_i}\left(\mathrm{e}^{\frac{V+R_sI}{\hat{a}_i}} - 1\right) - \frac{V + R_sI}{\hat{R}_{sh}},$$

and $RMSE = \sqrt{\sum_{i=1}^{N}\left[\hat{y}(t_i) - y(t_i)\right]^2/N}$.

Step 3: Calculate $ERR = \sum_{i=1}^{N}[\hat{y}(t_i) - y(t_i)]$. If $ERR > 0$, adjust $R_s = (R_s + R_s^{low})/2$. Otherwise, adjust $R_s = (R_s + R_s^{upp})/2$.

Step 4: Update R_s^{upp} and R_s^{low} according to the sign of ERR. If $ERR > 0$, $R_s^{upp} = R_s$, otherwise, $R_s^{low} = R_s$.

Step 5: If $RMSE$ is less than some tolerance or the iterative cycle reaches some preset number, stop the searching. Otherwise, update R_s^{upp} and R_s^{low} according to the sign of ERR and go back to *Step 2*.

F. Robustness enhancement

From the viewpoint of control theory, the transfer function (13) has a pole of $s = 1/a > 0$, which implies the system (14) is unstable. This is also true for the general case of multi-diode model. Identification for unstable system is not preferred because the convergence of the proposed algorithm might be sensitive to the accuracy of the integral calculation in such a case. To improve the robustness of the proposed algorithm, $\tilde{V}$ is introduced to yield a stable system.

In case of one-diode model, let $V = V_{oc} - \tilde{V}$, $0 \leq \tilde{V} \leq V_{oc}$, and $\tilde{x} = \tilde{V} - R_sI$, thus $x = V + R_sI = V_{oc} - (\tilde{V} - R_sI) = V_{oc} - \tilde{x}$. It follows from (7)-(9) that

$$\begin{aligned}
y &= I_L + I_o - \frac{V_{oc}}{R_{sh}} - I_o\mathrm{e}^{\frac{V_{oc}}{a}}\mathrm{e}^{-\frac{\tilde{x}}{a}} + \frac{\tilde{x}}{R_{sh}},\\
\frac{\mathrm{d}y}{\mathrm{d}\tilde{x}} &= \frac{I_o}{a}\mathrm{e}^{\frac{V_{oc}}{a}}\mathrm{e}^{-\frac{\tilde{x}}{a}} + \frac{1}{R_{sh}},\\
\frac{\mathrm{d}^2y}{\mathrm{d}\tilde{x}^2} &= -\frac{I_o}{a^2}\mathrm{e}^{\frac{V_{oc}}{a}}\mathrm{e}^{-\frac{\tilde{x}}{a}}.
\end{aligned}$$

Let $t = \tilde{x}$ and $u(t) \equiv 1$, by eliminating $\mathrm{e}^{-\tilde{x}/a}$ it gives

$$a\frac{\mathrm{d}^2y(t)}{\mathrm{d}t^2} + \frac{\mathrm{d}y(t)}{\mathrm{d}t} = \frac{u(t)}{R_{sh}}.$$

The corresponding transfer function is

$$G(s) = \frac{Y(s)}{U(s)} = \frac{ay(0)s^2 + [ay'(0) + y(0)]s + \frac{1}{R_{sh}}}{as^2 + s},$$

where $y(0) = I_L - I_o(\mathrm{e}^{V_{oc}/a} - 1) - V_{oc}/R_{sh}$, $y'(0) = I_o\mathrm{e}^{V_{oc}/a}/a + 1/R_{sh}$. In this way, the unstable pole $s = 1/a > 0$ becomes stable as $s = -1/a < 0$.

The remaining procedures are the same as aforementioned. Let $\phi(t) = \left[y(t), -u(t), -\int_{[0,t]}^{(1)} u(\tau), -\int_{[0,t]}^{(2)} u(\tau)\right]^T$, $\gamma(t) = -\int_{[0,t]}^{(1)} y(\tau)$, and

$$\theta = \begin{bmatrix} a \\ aI_L - aI_o(\mathrm{e}^{\frac{V_{oc}}{a}} - 1) - \frac{aV_{oc}}{R_{sh}} \\ I_L + I_o - \frac{V_{oc}-a}{R_{sh}} \\ \frac{1}{R_{sh}} \end{bmatrix},$$

the linear least square solution is $\theta = \left(\Phi^T\Phi\right)^{-1}\Phi^T\Gamma$ with $\Phi = [\phi(t_1), \phi(t_2), \cdots, \phi(t_N)]^T$ and $\Gamma = [\gamma(t_1), \gamma(t_2), \cdots, \gamma(t_N)]^T$. Once θ is determined, the parameters of one-diode model are obtained by $a = \theta_1$, $I_L = \theta_2/\theta_1 + (\theta_3 - \theta_2/\theta_1 - \theta_1\theta_4)(1 - \mathrm{e}^{-V_{oc}/\theta_1}) + V_{oc}\theta_4$, $I_o = (\theta_3 - \theta_2/\theta_1 - \theta_1\theta_4)/\mathrm{e}^{V_{oc}/\theta_1}$, and $R_{sh} = 1/\theta_4$.

In case of multi-diode model, with the same transform of $x = V_{oc} - \tilde{x}$, (15) becomes

$$y = I_L + \sum_{i=1}^{m} I_{o_i} - \sum_{i=1}^{m} I_{o_i} \mathrm{e}^{\frac{V_{oc}}{a_i}} \mathrm{e}^{-\frac{\tilde{x}}{a_i}} - \frac{V_{oc}}{R_{sh}} + \frac{\tilde{x}}{R_{sh}}. \quad (32)$$

Let $\tilde{a}_i = -a_i$, $\tilde{I}_L = I_L + \sum_{i=1}^{m} I_{o_i}(1 - \mathrm{e}^{V_{oc}/a_i}) - V_{oc}/R_{sh}$, $\tilde{I}_{o_i} = I_{o_i}\mathrm{e}^{V_{oc}/a_i}$, $\tilde{R}_{sh} = -R_{sh}$, and (32) is equivalent to

$$y = \tilde{I}_L + \sum_{i=1}^{m} \tilde{I}_{o_i} - \sum_{i=1}^{m} \tilde{I}_{o_i} \mathrm{e}^{\frac{\tilde{x}}{\tilde{a}_i}} - \frac{\tilde{x}}{\tilde{R}_{sh}},$$

which has the same format as (15). This means that all the derivation aforementioned are applicable to the parameter set $\{\tilde{a}_i, \tilde{I}_L, \tilde{I}_{o_i}, \tilde{R}_{sh}\}$. Once they are determined, the parameter set $\{a_i, I_L, I_{o_i}, R_{sh}\}$ is derived immediately by $a_i = -\tilde{a}_i$, $R_{sh} = -\tilde{R}_{sh}$, $I_{o_i} = \tilde{I}_{o_i}\mathrm{e}^{-V_{oc}/a_i}$, and $I_L = \tilde{I}_L - \sum_{i=1}^{m} I_{o_i}(1 - \mathrm{e}^{V_{oc}/a_i}) + V_{oc}/R_{sh}$.

IV. Validation

A. Indoor flash test

The I-V characteristics of full-sized commercial modules were measured indoor by a pulsed solar simulator (PASAN IIIB) with a constant illumination intensity plateau of about 12 ms used. The data acquisition, which requires about 10 ms, occurs during the plateau period, whereby the light intensity varies by less than $\pm 1\%$. The intensity of the solar simulator is calibrated with a c-Si reference cell certified by Fraunhofer ISE. The overall uncertainty of module power measurement is within $\pm 2\%$.

Example 1 (c-Si modules): The I-V characteristic of a crystalline PV module from the indoor flash test under STC (1000 W/m^2, 25°C) is shown in Fig.2. Both one-diode and two-diode models are considered for this case study.

1) One-diode model. Firstly, use the last 10 points at OC to derive a linear fitting: $I = kV + p$, where $k = -0.9131$. $R_s^{upp} \approx -1/k = 1.0952$. $R_s^{low} = 0$. Arbitrarily choose $R_s \in [R_s^{low}, R_s^{upp}]$, e.g., $R_s = 1.0952$, and follow the proposed integral-based linear identification presented in Section III-A, R_s converges to $R_s = 0.655$ after about 30 steps with the proposed binary searching, as shown in Fig.3. Multiple integrals from (27) are estimated by the numerical integration presented in Section III-D. It follows from (29) that $\theta_1 = 1.9891$, $\theta_2 = 9.8295$, $\theta_3 = 4.9434$, $\theta_4 = 8.9631 \times 10^{-4}$. Thus, $a = \theta_1 = 1.9891$ V, $I_L = \theta_2/\theta_1 = 4.9416$ A, $I_o = \theta_3 - \theta_2/\theta_1 - \theta_1\theta_4 = 4.1785 \times 10^{-9}$ A, and $R_{sh} = 1/\theta_4 = 1.1157 \times 10^3\ \Omega$.

Fig.2 also shows the comparison between the I-V curves from the real measurement and the one-code model, where the average absolute error $\bar{E} = 1/N \sum_{i=1}^{N} |ERR| = 0.0085$. The $RMSE$ is shown in Fig.3, which converges to 1.67% at last after 35 steps with Tol = 2%.

2) Two-diode model. It is clear to see from Fig.2 that one-diode model is good enough to represent the whole I-V curve accurately. This implies that if two-diode model is applied, $I_{o_2} \to 0$, which will cause a singular matrix in the identification of Section III-B. To avoid such a potential problem, robustness enhancement discussed in Section III-F will be applied. With $m = 2$, (32) becomes

$$y = I_L + I_{o_1}\left(1 - \mathrm{e}^{\frac{V_{oc}-\tilde{x}}{a_1}}\right) + I_{o_2}\left(1 - \mathrm{e}^{\frac{V_{oc}-\tilde{x}}{a_2}}\right) - \frac{V_{oc} - \tilde{x}}{R_{sh}},$$

where $\tilde{x} = \tilde{V} - R_s I$, $\tilde{V} = V_{oc} - V$. And its multiple differentials are

$$\frac{\mathrm{d}y}{\mathrm{d}\tilde{x}} = \frac{I_{o_1}}{a_1}\mathrm{e}^{\frac{V_{oc}-\tilde{x}}{a_1}} + \frac{I_{o_2}}{a_2}\mathrm{e}^{\frac{V_{oc}-\tilde{x}}{a_2}} + \frac{1}{R_{sh}}, \quad (33)$$

$$\frac{\mathrm{d}^2y}{\mathrm{d}\tilde{x}^2} = -\frac{I_{o_1}}{a_1^2}\mathrm{e}^{\frac{V_{oc}-\tilde{x}}{a_1}} - \frac{I_{o_2}}{a_2^2}\mathrm{e}^{\frac{V_{oc}-\tilde{x}}{a_2}}, \quad (34)$$

$$\frac{\mathrm{d}^3y}{\mathrm{d}\tilde{x}^3} = \frac{I_{o_1}}{a_1^3}\mathrm{e}^{\frac{V_{oc}-\tilde{x}}{a_1}} + \frac{I_{o_2}}{a_2^3}\mathrm{e}^{\frac{V_{oc}-\tilde{x}}{a_2}}. \quad (35)$$

(34) and (35) in matrix format are

$$\begin{bmatrix} \frac{\mathrm{d}^2y}{\mathrm{d}\tilde{x}^2} \\ \frac{\mathrm{d}^3y}{\mathrm{d}\tilde{x}^3} \end{bmatrix} = \begin{bmatrix} -\frac{I_{o_1}}{a_1^2} & -\frac{I_{o_2}}{a_2^2} \\ \frac{I_{o_1}}{a_1^3} & \frac{I_{o_2}}{a_2^3} \end{bmatrix} \begin{bmatrix} \mathrm{e}^{\frac{V_{oc}-\tilde{x}}{a_1}} \\ \mathrm{e}^{\frac{V_{oc}-\tilde{x}}{a_2}} \end{bmatrix}.$$

Thus,

$$\begin{bmatrix} \mathrm{e}^{\frac{V_{oc}-\tilde{x}}{a_1}} \\ \mathrm{e}^{\frac{V_{oc}-\tilde{x}}{a_2}} \end{bmatrix} = \begin{bmatrix} -\frac{I_{o_1}}{a_1^2} & -\frac{I_{o_2}}{a_2^2} \\ \frac{I_{o_1}}{a_1^3} & \frac{I_{o_2}}{a_2^3} \end{bmatrix}^{-1} \begin{bmatrix} \frac{\mathrm{d}^2y}{\mathrm{d}\tilde{x}^2} \\ \frac{\mathrm{d}^3y}{\mathrm{d}\tilde{x}^3} \end{bmatrix} = \begin{bmatrix} \frac{a_1^3}{I_{o_1}(a_2-a_1)} & \frac{a_1^3 a_2}{I_{o_1}(a_2-a_1)} \\ -\frac{a_2^3}{I_{o_2}(a_2-a_1)} & -\frac{a_1 a_2^3}{I_{o_2}(a_2-a_1)} \end{bmatrix} \begin{bmatrix} \frac{\mathrm{d}^2y}{\mathrm{d}\tilde{x}^2} \\ \frac{\mathrm{d}^3y}{\mathrm{d}\tilde{x}^3} \end{bmatrix}.$$

Substitute it into (33), it yields

$$a_1 a_2 \frac{\mathrm{d}^3y(t)}{\mathrm{d}t^3} + (a_1 + a_2)\frac{\mathrm{d}^2y(t)}{\mathrm{d}t^2} + \frac{\mathrm{d}y(t)}{\mathrm{d}t} = \frac{u(t)}{R_{sh}}, \quad (36)$$

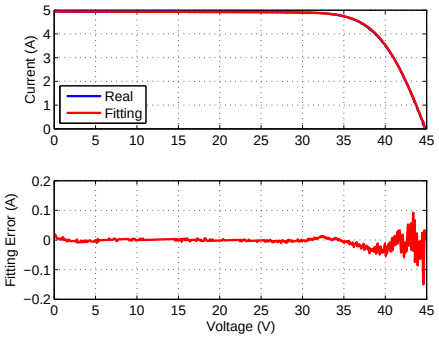

Fig. 2. Accuracy of the proposed method for c-Si module

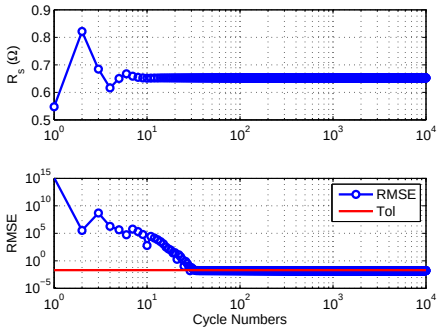

Fig. 3. Convergence of R_s and $RMSE$ for c-Si module

where $t = \tilde{x}$ and $u(t) \equiv 0$. After Laplace transform, (36) becomes

$$a_1a_2\left[s^3Y(s) - y''(0) - sy'(0) - s^2y(0)\right] + (a_1+a_2)\times$$
$$\left[s^2Y(s) - y'(0) - sy(0)\right] + \left[sY(s) - y(0)\right] = \frac{U(s)}{R_{sh}}, \quad (37)$$

where

$$y(0) = I_L + I_{o_1}\left(1 - \mathrm{e}^{\frac{V_{oc}}{a_1}}\right) + I_{o_2}\left(1 - \mathrm{e}^{\frac{V_{oc}}{a_2}}\right) - \frac{V_{oc}}{R_{sh}}, \quad (38)$$

$$y'(0) = \frac{I_{o_1}}{a_1}\mathrm{e}^{\frac{V_{oc}}{a_1}} + \frac{I_{o_2}}{a_2}\mathrm{e}^{\frac{V_{oc}}{a_2}} + \frac{1}{R_{sh}}, \quad (39)$$

$$y''(0) = -\frac{I_{o_1}}{a_1^2}\mathrm{e}^{\frac{V_{oc}}{a_1}} - \frac{I_{o_2}}{a_2}\mathrm{e}^{\frac{V_{oc}}{a_2}}. \quad (40)$$

Utilize $sU(s) = 1$, and (37) is equivalent to

$$a_1a_2s^3Y(s) + (a_1+a_2)s^2Y(s) - a_1a_2y(0)s^3U(s) -$$
$$\left[a_1a_2y'(0) + (a_1+a_2)y(0)\right]s^2U(s) - \frac{U(s)}{R_{sh}} -$$
$$\left[a_1a_2y''(0) + (a_1+a_2)y'(0) + y(0)\right]sU(s) = -sY(s).$$

Therefore, the differential equation representation with zero initial conditions are

$$a_1a_2\frac{\mathrm{d}^3y(t)}{\mathrm{d}t^3} + (a_1+a_2)\frac{\mathrm{d}^2y(t)}{\mathrm{d}t^2} - a_1a_2y(0)\frac{\mathrm{d}^3u(t)}{dt^3} -$$
$$\left[a_1a_2y'(0) + (a_1+a_2)y(0)\right]\frac{\mathrm{d}^2u(t)}{\mathrm{d}t^2} - \frac{u(t)}{R_{sh}} -$$
$$\left[a_1a_2y''(0) + (a_1+a_2)y'(0) + y(0)\right]\frac{\mathrm{d}u(t)}{\mathrm{d}t} = -\frac{\mathrm{d}y(t)}{\mathrm{d}t}. \quad (41)$$

Apply triple integral (27) (with $n = 3$) to (41), we have

$$a_1a_2y(t) + (a_1+a_2)\int_{[0,t]}^{(1)} y(\tau) - a_1a_2y(0)u(t)$$
$$- \left[a_1a_2y'(0) + (a_1+a_2)y(0)\right]\int_{[0,t]}^{(1)} u(\tau)$$
$$- \left[a_1a_2y''(0) + (a_1+a_2)y'(0) + y(0)\right]\int_{[0,t]}^{(2)} u(\tau)$$
$$- \frac{1}{R_{sh}}\int_{[0,t]}^{(3)} u(\tau) = -\int_{[0,t]}^{(2)} y(\tau). \quad (42)$$

Let $\gamma(t) = -\int_{[0,t]}^{(2)} y(\tau)$, $\phi(t) = [y(t), \int_{[0,t]}^{(1)} y(\tau), -u(t), -\int_{[0,t]}^{(1)} u(\tau), -\int_{[0,t]}^{(2)} u(\tau), -\int_{[0,t]}^{(3)} u(\tau)]^T$, and

$$\theta := \begin{bmatrix} \theta_1 \\ \theta_2 \\ \theta_3 \\ \theta_4 \\ \theta_5 \\ \theta_6 \end{bmatrix} = \begin{bmatrix} a_1a_2 \\ a_1+a_2 \\ \theta_1y(0) \\ \theta_1y'(0) + \theta_2y(0) \\ \theta_1y''(0) + \theta_2y'(0) + y(0) \\ \frac{1}{R_{sh}} \end{bmatrix}, \quad (43)$$

then (42) can be rewritten in matrix format of $\phi(t)^T\theta = \gamma(t)$. The linear least solution to θ is given by (30). Immediately, $R_{sh} = 1/\theta_6$, $a_{1,2} = (\theta_2 \pm \sqrt{\theta_2^2 - 4\theta_1})/2$, and

$$\begin{bmatrix} \theta_3 \\ \theta_4 \\ \theta_5 \end{bmatrix} = \begin{bmatrix} \theta_1 & 0 & 0 \\ \theta_2 & \theta_1 & 0 \\ 1 & \theta_2 & \theta_1 \end{bmatrix}\begin{bmatrix} y(0) \\ y'(0) \\ y''(0) \end{bmatrix}.$$

Therefore,

$$\begin{bmatrix} y(0) \\ y'(0) \\ y''(0) \end{bmatrix} = \begin{bmatrix} \theta_1 & 0 & 0 \\ \theta_2 & \theta_1 & 0 \\ 1 & \theta_2 & \theta_1 \end{bmatrix}^{-1}\begin{bmatrix} \theta_3 \\ \theta_4 \\ \theta_5 \end{bmatrix}.$$

It follows from (38)-(40) that

$$\begin{bmatrix} y(0) + \frac{V_{oc}}{R_{sh}} \\ y'(0) - \frac{1}{R_{sh}} \\ y''(0) \end{bmatrix} = \begin{bmatrix} 1 & 1 - \mathrm{e}^{\frac{V_{oc}}{a_1}} & 1 - \mathrm{e}^{\frac{V_{oc}}{a_2}} \\ 0 & \frac{\mathrm{e}^{\frac{V_{oc}}{a_1}}}{a_1} & \frac{\mathrm{e}^{\frac{V_{oc}}{a_2}}}{a_2} \\ 0 & -\frac{\mathrm{e}^{\frac{V_{oc}}{a_1}}}{a_1^2} & -\frac{\mathrm{e}^{\frac{V_{oc}}{a_2}}}{a_2^2} \end{bmatrix}\begin{bmatrix} I_L \\ I_{o_1} \\ I_{o_2} \end{bmatrix}.$$

Thus,

$$\begin{bmatrix} I_L \\ I_{o_1} \\ I_{o_2} \end{bmatrix} = \begin{bmatrix} 1 & 1 - \mathrm{e}^{\frac{V_{oc}}{a_1}} & 1 - \mathrm{e}^{\frac{V_{oc}}{a_2}} \\ 0 & \frac{\mathrm{e}^{\frac{V_{oc}}{a_1}}}{a_1} & \frac{\mathrm{e}^{\frac{V_{oc}}{a_2}}}{a_2} \\ 0 & -\frac{\mathrm{e}^{\frac{V_{oc}}{a_1}}}{a_1^2} & -\frac{\mathrm{e}^{\frac{V_{oc}}{a_2}}}{a_2^2} \end{bmatrix}^{-1}\begin{bmatrix} y(0) + \frac{V_{oc}}{R_{sh}} \\ y'(0) - \frac{1}{R_{sh}} \\ y''(0) \end{bmatrix}.$$

In this way, with the same I-V characteristics data as shown in Fig.2, we got $\theta_1 = 0.6849$, $\theta_2 = 2.2356$, $\theta_3 = 0.0247$, $\theta_4 = 3.3348$, $\theta_5 = 4.9034$, $\theta_6 = 0.0010$. The two-diode model parameters are identified as $a_1 = 1.8691$ V, $a_2 = 0.3664$ V, $I_{o_1} = 1.5168 \times 10^{-10}$ A, $I_{o_2} = 7.9060 \times 10^{-54}$ A, $I_L = 4.9480$ A, $R_{sh} = 955.1229\ \Omega$, and $R_s = 0.6845\ \Omega$. The average absolute error $\bar{E} = 0.0080$ and $RMSE = 1.35\%$, both of which are slightly reduced as compared to the one-diode model result. As expected, I_{o_2} is indeed extremely close to zero, whereas other parameters are comparable to their counter parts in one-diode model result.

It should be highlighted that the diode model parameters derived from the indoor flash test are not constant. Actually, they are varying with temperature and solar radiation. Therefore, it is necessary to check the online computability of the proposed method for PV modules under non-constant environment, which is demonstrated by the outdoor module testing as follows.

B. Outdoor module testing

Outdoor module testing (OMT) is usually carried out by many PV panel manufacturers and solar research institutes for the module performance evaluation under the real operating environments. DC parameters including full I-V curves, V_{oc}, I_{sc}, V_{mpp}, I_{mpp}, P_{mpp} together with module temperature are measured and logged every minute. Environmental parameters including in-plane solar irradiance G_{si}, ambient temperature T_{amb}, module temperature T_{mod}, wind speed and wind direction are logged simultaneously with the DC parameters. Between I-V measurements, electrical energy is maintained at the module maximum power point (MPP). The uncertainty of all electrical measured parameters is within $\pm 0.1\%$ for full scale. With these I-V data in time series, the diode model parameters can be identified online by the proposed method and correlated to the environmental factors like irradiance, temperature, etc.

Fig.4 shows the time series of G_{si}, T_{amb} and T_{mod} on a typical day from the OMT testbed of Solar Energy Research Institute of Singapore (SERIS). The plot is centred around the solar noon, which was at 13:10 on the 5 August 2010.

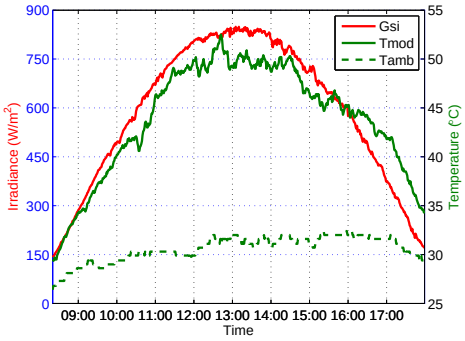

Fig. 4. Environmental factors of a typical day in SERIS' OMT testbed

By applying the proposed method in Section III, the time-varying one-diode model parameters I_L, I_o, a, R_s and R_{sh} for the same day are identified, as shown in Fig.5. The variation of the identified parameters reflects the dynamics of the PV module under different environmental conditions, which cannot be seen from the static I-V curves.

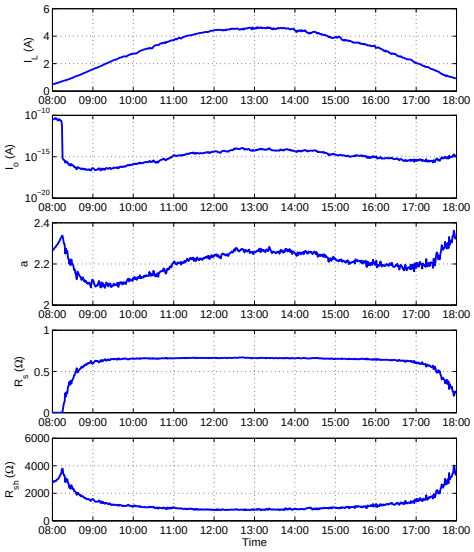

Fig. 5. Identified one-diode model parameters

The relationships between the identified parameters and the environmental operating conditions are further illustrated in Fig.6-9. A proportional relationship between I_L and irradiance intensity is observed in Fig.6. It is also apparent from Fig.7 that I_o generally shows an increasing trend with rising module temperature. This also agrees with the theoretical temperature dependence of I_o, as given by $I_o = BT^3 \mathrm{e}^{-E_g/(kT)}$, where E_g is the band gap of silicon and B is a temperature independent constant [13]. Fig.8 illustrates that a generally decreases with increasing irradiance for $G_{si} < 300$ W/m^2 and increases beyond that, which is as reported in [38]. When irradiance decreases in Fig.9, the series resistance R_s decreases and the shunt resistance R_{sh} increases, which is consistent with previous reported results [39]. The decrease in R_s is due to the decreased thermal loss (I^2R_s) with decreasing irradiance.

The RMSE of the proposed algorithm in OMT case is

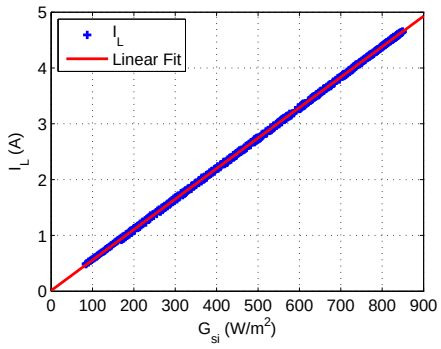

Fig. 6. Proportional relationship between I_L and G_{si}

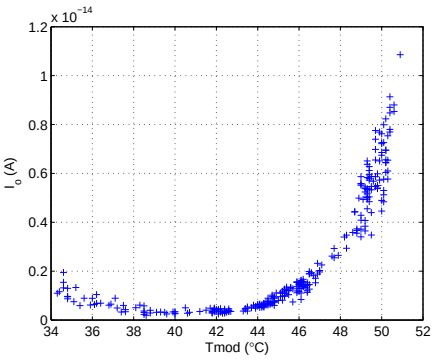

Fig. 7. Relationship between I_o and T_{mod}

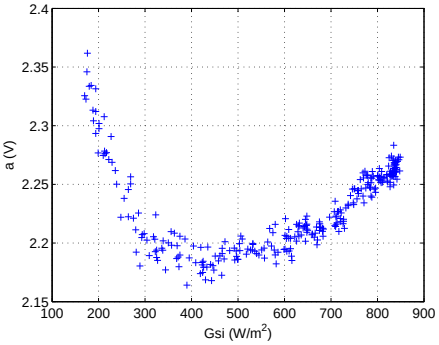

Fig. 8. Relationship between a and G_{si}

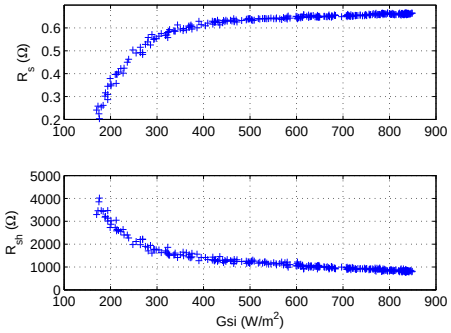

Fig. 9. Relationship between R_s, R_sh and G_{si}

shown in Fig.10, where the burden of the online calculation for convergence (iterative steps for R_s until Tol or maximum cycle is achieved) is presented as well. Among 600 plus I-V scans during the day, there are only three cases with the RMSE exceeding the preset 1% Tol when the maximum number (100) of steps is reached. Even for these three cases, the RMSE is still below 1.5%. The iterative steps are very stable, and they are usually less than 30. This indicates that the online calculation burden of the proposed algorithm is low and the identification can be done by an industrial PC locally between two consecutive I-V scan (1 min in our case).

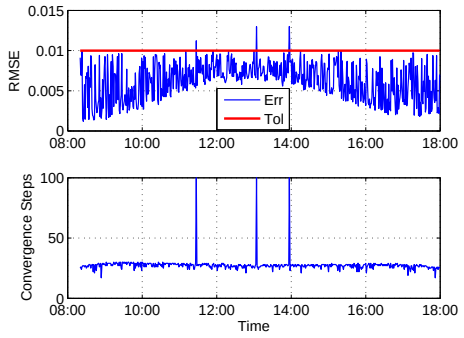

Fig. 10. RMSE and burden of online calculation

V. Comparison with other methods

As mentioned in the Introduction, the recent progress in the parameter identification of diode model are mainly from Laudani *et al.* [15], [34], and the evolutionary algorithms [29], [30]. In this section, the comparison of the proposed method with these two approaches are discussed.

A. Laudani's method

In [34], two data sets of I-V curves (26 points) are presented, which are initially proposed in [40] and are commonly used to test the effectiveness of the extraction algorithms. One refers to a solar module (Photowatt-PWP 201) at 45°C and the other refers to a solar cell (c-Si) at 33°C. The one-diode model parameters I_L, I_o and R_{sh} are proved to be functions of R_s and a. So the searching in the two-dimensional parameter space of R_s and a with the constrained conditions of (2), (3) and (5) yields Solution A; with the constrained conditions of (2), (3) and (4) yields Solution B. These two solutions are then fine tuned as the initial values of some nonlinear least square for the experimental data, which yields Solution C and D, respectively.

With the solar module I-V data in [34], the comparison of the solutions of one-diode model by the propose and Laudani's method are shown in TABLE I, where "MAE" is the mean absolute error and "Step" is the number of iterative searching cycle before convergence. It is clear to see that the proposed method is very close to the model parameters values in Laudani's results. Although the error is slightly bigger, the number of iteration steps is less.

The error mainly arises from the numerical integrations presented in Section III-D and the few I-V data samples available (26 points only). If more data samples on the I-V curve are known, the error of the proposed method will be reduced. To illustrate this point, model parameters from the solution of Laudani 1D was used to reproduce the whole I-V curve with the help of (6). The number of samples are selected to be 50, 100, 200. Based on such samples on the I-V curve derived from Laudani 1D solution, the RMSE of the proposed method to the whole I-V and the experimental data are shown in TABLE II. As expected, the more data samples, the smaller RMSE. When data samples increased to 100, the RMSE for the experimental data is already better than the solutions of Laudani 1A/B and all the other results compared in [34].

TABLE II
RMSE WITH DIFFERENT DATA SAMPLES (MODULE)

Source	Solutions	RMSE[1]	RMSE[2]	Steps
Module[3]	From 50 pts	3.3085×10^{-4}	2.2290×10^{-3}	8
	From 100 pts	8.5583×10^{-5}	2.0939×10^{-3}	13
	From 200 pts	2.0177×10^{-5}	2.0874×10^{-3}	12
Cell[4]	From 50 pts	3.6098×10^{-4}	9.9881×10^{-4}	8
	From 100 pts	8.8401×10^{-5}	8.6810×10^{-4}	9
	From 200 pts	2.2234×10^{-5}	8.5153×10^{-4}	10

[1] for the whole I-V curve [2] for the experimental data in [34]
[3] I-V curve is produced from Laudani 1D
[4] I-V curve is produced from Laudani 2D

The result comparison for the solar cell I-V data in [34] is shown in TABLE III. The RMSE of the proposed method is smaller than the results of Laudani 2A/C, and only slightly bigger than Laudani 2B/D. When data samples increased to 100, the proposed method already outperformed Laudani 2B, as shown in TABLE II.

In general, Laudani's method has many benefits in two aspects: 1) it utilizes the Lambert W function to convert a non-concave optimal problem into a concave optimal problem; 2) it utilizes reduced forms to decrease the dimension of the parameter space from five to two. It can deal with the I-V data from the data sheet (points at SC, OC, MPP) or experiment (full I-V curve), and in most of cases, it yields the best results in terms of RMSE and/or MAE. The deficiencies of Laudani's method may be: 1) no unique solutions; 2) inapplicable to the multi-diode model ($m > 1$) parameter identification due to the limitations of Lambert W function; 3) not easy to be implemented and unsuitable for online parameter identification.

The proposed method further reduces the dimension of the parameter space to one. It uses linear square other than nonlinear optimal algorithms to derive diode model parameters, so the drawbacks of nonlinear algorithms are avoided. It can also be used for multiple-diode model and simple enough to be implemented as online calculation. The deficiencies is that it requires the knowledge of the full I-V curve data.

B. Evolution algorithms

As mentioned in the Introduction, evolution algorithms are very suitable for the search of a global optimal solution. Recently, two types of evolution algorithms using differential evolution (DE) [29] and genetic algorithm (GA) [30] yield

TABLE I
SOLUTION COMPARISON FOR SOLAR MODULE

Solutions	I_L (A)	I_o (μA)	R_s (Ω)	R_{sh} (kΩ)	a (N_snkT_c/q)	RMSE	MAE	Steps
The proposed	1.0334262	2.4424001	1.2307473	0.6034037	1.2975122	2.4777×10^{-3}	1.8461×10^{-3}	8
Laudani 1A	1.032173	3.035367	1.218407	0.783516	1.319345	2.1176×10^{-3}	1.6425×10^{-3}	12
Laudani 1B	1.033537	2.825571	1.224053	0.689321	1.312115	2.1547×10^{-3}	1.6060×10^{-3}	10
Laudani 1C	1.0323759	2.5188885	1.2390187	0.7456443	1.3002458	2.0465×10^{-3}	1.6917×10^{-3}	19
Laudani 1D	1.0323759	2.5188848	1.2390187	0.7456431	1.3002456	2.0465×10^{-3}	1.6917×10^{-3}	28

TABLE III
SOLUTION COMPARISON FOR SOLAR CELL

Solutions	I_L (A)	I_o (μA)	R_s (Ω)	R_{sh} (Ω)	a (N_snkT_c/q)	RMSE	MAE	Steps
The proposed	0.7609438	0.3456572	3.614233×10^{-2}	49.482205	3.9256187×10^{-2}	1.0548×10^{-3}	8.5202×10^{-4}	8
Laudani 2A	0.764114	3.496×10^{-3}	4.5438×10^{-2}	11.103851	2.9929942×10^{-2}	1.1388×10^{-2}	9.4014×10^{-3}	8
Laudani 2B	0.761060	0.290125	3.6800×10^{-2}	49.973561	3.8784080×10^{-2}	8.8437×10^{-4}	6.9732×10^{-4}	7
Laudani 2C	0.7706871	3.668522×10^{-3}	4.911298×10^{-2}	11.103904	2.997888×10^{-2}	8.9605×10^{-3}	7.2064×10^{-3}	14
Laudani 2D	0.7607884	0.3102482	3.655304×10^{-2}	52.859056	3.8965248×10^{-2}	7.7301×10^{-4}	6.7810×10^{-4}	16

good results for diode model parameter identification. Hence, it is worthy to compare the proposed method with them.

Since no full I-V curve data are provided in [29], [30], we do the comparison in an indirect way as follows. Firstly, use the identified parameters (I_L, I_o, a, R_s and R_{sh}) to reconstruct the I-V curve by (6); Secondly, use that I-V curve data to identify diode-model parameters with the proposed method. Since DE and GA are applied to derive a, R_s and R_{sh} only (I_L and I_o are derived by formulas in [6], [32]), we only compare the results of a, R_s and R_{sh}. TABLE IV shows the results of a, R_s and R_{sh} from the proposed method and DE/GA. It is clear to see that the differences in between are very minor.

TABLE IV
SOLUTION COMPARISON WITH EVOLUTION ALGORITHMS

Module	Solutions	a (N_snkT_c/q)	R_s (Ω)	R_{sh} (Ω)
Shell SM55	Proposed	1.2666	0.3001	2.3165×10^{3}
(mono-cSi)	DE	1.2665	0.3	2.34×10^{3}
Shell S75	Proposed	1.2300	0.2000	1.7834×10^{3}
(multi-cSi)	DE	1.2295	0.2	1.79×10^{3}
Sanyo 215	Proposed	2.1778	0.7821	851.2464
(HIT)	GA	2.1780	0.782	852.177
Kyocera 200	Proposed	1.5340	0.3310	882.7933
(multi-cSi)	GA	1.5337	0.331	883.925

The result of the two-diode model for the aforementioned Kyocera module (Kyocera - KC200GT) was also reported in [30]. It is interesting to comparing this result with ours. If looking carefully at the comparison shown in TABLE V, the GA algorithm gives comparable I_{o_1} and I_{o_2} (both in 10^{-9} A). a_1 and a_2 are also near to each other. If ignoring the differences between them, the two-diode can be combined as one. This implies that GA algorithm actually gives a result of one-diode model but mathematically divides it into two diodes format with no physical meaning. That's a common issue for the global optimization algorithm like DE and GA, whereas the proposed method has no such problems.

TABLE V
COMPARISON OF TWO-DIODE MODELS

Parameters	GA	Proposed
a_1 (V)	1.5420	1.4936
a_2 (V)	1.9095	0.4944
R_s (Ω)	0.29	0.4095
R_{sh} (Ω)	480.496	842.8287
I_{o_1} (A)	4.23×10^{-9}	1.6044×10^{-9}
I_{o_2} (A)	9.1478×10^{-9}	2.6559×10^{-29}
MAE	0.02	0.0058

VI. CONCLUSION

A novel method is proposed in this paper to identify all the one-diode model parameters of PV panels from a single I-V curve. By utilizing the mapping of transfer function, the nonlinear fitting problem is converted equivalently to a linear system identification. Correspondingly, the dimension of the parameter space is reduced from five to one. Indoor and outdoor module testing show its effectiveness and online computability, and its accuracy is also comparable to or better than the best results from the literature.

APPENDIX A
PROOF OF LEMMA 1

Consider the general case of multi-diode model with

$$\Phi = [\phi(t_1), \phi(t_2), \cdots, \phi(t_N)]^T := [\Phi_1, \Phi_2],$$

$$\Phi_1 = \begin{bmatrix} y(t_1) & \int^{(1)}_{[0,t_1]} y(\tau) & \cdots & \int^{(m-1)}_{[0,t_1]} y(\tau) \\ y(t_2) & \int^{(1)}_{[0,t_2]} y(\tau) & \cdots & \int^{(m-1)}_{[0,t_2]} y(\tau) \\ \vdots & \vdots & \ddots & \vdots \\ y(t_N) & \int^{(1)}_{[0,t_N]} y(\tau) & \cdots & \int^{(m-1)}_{[0,t_N]} y(\tau) \end{bmatrix} := [\phi_{i,j}],$$

$$\Phi_2 = -\begin{bmatrix} u(t_1) & \int_{[0,t_1]}^{(1)} u(\tau) & \cdots & \int_{[0,t_1]}^{(m+1)} u(\tau) \\ u(t_2) & \int_{[0,t_2]}^{(1)} u(\tau) & \cdots & \int_{[0,t_2]}^{(m+1)} u(\tau) \\ \vdots & \vdots & \ddots & \vdots \\ u(t_N) & \int_{[0,t_N]}^{(1)} u(\tau) & \cdots & \int_{[0,t_N]}^{(m+1)} u(\tau) \end{bmatrix} =: [\varphi_{i,l}].$$

Recall from (15) that

$$y(t) = I_L + \sum_{i=1}^{m} I_{o_i} - \sum_{i=1}^{m} I_{o_i} \mathrm{e}^{\frac{t}{a_i}} - \frac{t}{R_{sh}},$$

and $u(t) \equiv 1$ by the definition. For $i = 1, 2, \cdots, N$,

$$\begin{aligned} \phi_{i,j} &= \int_{[0,t_i]}^{(j-1)} y(\tau) = \frac{I_L + \sum_{i=1}^{m} I_{o_i}}{(j-1)!} t_i^{j-1} - \frac{t_i^j}{j! R_{sh}} \\ &\quad + \sum_{k=0}^{j-2} \sum_{l=1}^{m} I_{o_l} a_l^{j-k-1} \frac{t_i^k}{k!} - \sum_{k=1}^{j} I_{o_k} a_k^{j-1} \mathrm{e}^{\frac{t_i}{a_k}}, \\ \varphi_{i,l} &= -\int_{[0,t_i]}^{(l-1)} u(\tau) = -\frac{1}{j!} t_i^l, \end{aligned}$$

where $j = 1, 2, \cdots, m$ and $l = 1, 2, \cdots, m+2$. After elementary column operations for Φ, $\Phi_1 \to \tilde{\Phi}_1 := [\tilde{\phi}_{i,j}]$ with

$$\tilde{\phi}_{i,j} = \sum_{k=1}^{j} I_{o_k} a_k^{j-1} \mathrm{e}^{\frac{t_i}{a_k}}.$$

In matrix format,

$$\tilde{\Phi}_1 = \underbrace{\begin{bmatrix} \mathrm{e}^{\frac{t_1}{a_1}} & \mathrm{e}^{\frac{t_1}{a_2}} & \cdots & \mathrm{e}^{\frac{t_1}{a_m}} \\ \mathrm{e}^{\frac{t_2}{a_1}} & \mathrm{e}^{\frac{t_2}{a_2}} & \cdots & \mathrm{e}^{\frac{t_2}{a_m}} \\ \vdots & \vdots & \ddots & \vdots \\ \mathrm{e}^{\frac{t_N}{a_1}} & \mathrm{e}^{\frac{t_N}{a_2}} & \cdots & \mathrm{e}^{\frac{t_N}{a_m}} \end{bmatrix}}_{E} \times$$

$$\underbrace{\begin{bmatrix} I_{o_1} & & & \\ & I_{o_2} & & \\ & & \ddots & \\ & & & I_{o_m} \end{bmatrix}}_{\Lambda} \underbrace{\begin{bmatrix} 1 & a_1 & \cdots & a_1^{m-1} \\ 1 & a_2 & \cdots & a_2^{m-1} \\ \vdots & \vdots & \ddots & \vdots \\ 1 & a_m & \cdots & a_m^{m-1} \end{bmatrix}}_{V^*}.$$

Since Λ is diagonal and V^* is a standard Vandermonde matrix, $\mathrm{rank}(\Lambda) = \mathrm{rank}(V^*) = m$. If $t_2 - t_1 = t_3 - t_2 = \cdots = t_m - t_{m-1} = T_s > 0$, as $N \geq 2m+2$, the first m row of E

$$E_m = \begin{bmatrix} 1 & 1 & \cdots & 1 \\ \mathrm{e}^{\frac{T_s}{a_1}} & \mathrm{e}^{\frac{T_s}{a_2}} & \cdots & \mathrm{e}^{\frac{T_s}{a_m}} \\ \vdots & \vdots & \ddots & \vdots \\ (\mathrm{e}^{\frac{T_s}{a_1}})^{n-1} & (\mathrm{e}^{\frac{T_s}{a_2}})^{n-1} & \cdots & (\mathrm{e}^{\frac{T_s}{a_m}})^{m-1} \end{bmatrix} \times \begin{bmatrix} \mathrm{e}^{\frac{t_1}{a_1}} & & & \\ & \mathrm{e}^{\frac{t_1}{a_2}} & & \\ & & \ddots & \\ & & & \mathrm{e}^{\frac{t_1}{a_m}} \end{bmatrix},$$

so $\mathrm{rank}(E) = \mathrm{rank}(E_m) = m$. Otherwise, it is always possible to find some ΔT such that $t_i = n_i \Delta T$, $n_i \in \mathbb{N}$ for $i = 1, 2, \cdots, m$. Construct matrix

$$E^* = \begin{bmatrix} 1 & 1 & \cdots & 1 \\ \mathrm{e}^{\frac{\Delta T}{a_1}} & \mathrm{e}^{\frac{\Delta T}{a_2}} & \cdots & \mathrm{e}^{\frac{\Delta T}{a_m}} \\ \vdots & \vdots & \ddots & \vdots \\ \mathrm{e}^{\frac{n_m \Delta T}{a_1}} & \mathrm{e}^{\frac{n_m \Delta T}{a_2}} & \cdots & \mathrm{e}^{\frac{n_m \Delta T}{a_m}} \end{bmatrix} \in \mathbb{R}_{n_m \times n},$$

and E_m is sub-matrix of E^*. Since E^* is a Vandermonde matrix with full column rank, $\mathrm{rank}(E) = \mathrm{rank}(E_m) = \mathrm{rank}(E^*) = m$. So, Φ_1 is full column rank, i.e., $\mathrm{rank}(\Phi_1) = m$.

$$\Phi_2 = \underbrace{\begin{bmatrix} t_1 & t_1^2 & \cdots & t_1^{m+2} \\ t_2 & t_2^2 & \cdots & t_2^{m+2} \\ \vdots & \vdots & \ddots & \vdots \\ t_N & t_N^2 & \cdots & t_N^{m+2} \end{bmatrix}}_{V_2} \times$$

$$\begin{bmatrix} -1 & & & \\ & \ddots & & \\ & & \frac{-1}{(m+1)!} & \\ & & & \frac{-1}{(m+2)!} \end{bmatrix}$$

As $N \geq 2m+2$, the first $m+2$ row of V_2 is a Vandermonde matrix, so $\mathrm{rank}(\Phi_2) = \mathrm{rank}(V_2) = m+2$, i.e., Φ_2 is full column rank. Since $\Phi = [\Phi_1, \Phi_2]$ with the full column rank of both Φ_1 and Φ_2, Φ is also full column rank. $N \geq 2m+2$ implies that the row number of Φ is no less than the column number. So, $\mathrm{rank}(\Phi) = 2m+2$ and $\Phi^T \Phi$ is full rank, i.e., $(\Phi^T \Phi)^{-1}$ exists.

REFERENCES

[1] J. S. C. M. Raj and A. E. Jeyakumar, "A novel maximum power point tracking technique for photovoltaic module based on power plane analysis of *I-V* characteristics," *IEEE Trans. Ind. Electron.*, vol. 61, no. 9, pp. 4734–4745, 2014.

[2] J. J. Soon, K.-S. Low, and S. T. Goh, "Multi-dimension diode photovoltaic (PV) model for different PV cell technologies," in *IEEE 23rd ISIE*, 2014, pp. 2496–2501.

[3] B. G. Streetman and S. Banerjee, *Solid state electronic devices*, 5th ed. New Jersey: Prentice Hall, 2000.

[4] K. R. McIntosh, "Lumps, humps and bumps: three detrimental effects in the current-voltage curve of silicon solar cells," Ph.D. dissertation, University of New South Wales, 2001.

[5] D. Macdonald and A. Cuevas, "Reduced fill factors in multicrystalline silicon solar cells due to injection-level dependent bulk recombination lifetime," *Prog. Photovolt: Res. Appl.*, no. 8, pp. 363–375, 2000.

[6] W. De Soto, S. Klein, and W. Beckman, "Improvement and validation of a model for photovoltaic array performance," *Sol. Energy*, vol. 80, no. 1, pp. 78–88, 2006.

[7] F. Pelanchon, P. Mialhe, and J. Charles, "The photocurrent and the open-circuit voltage of a silicon solar cell," *Sol. Cells*, vol. 28, no. 1, pp. 41–55, 1990.

[8] N. Ravindra and B. Prasad, "Saturation current in solar cells: an analysis," *Sol. Cells*, vol. 2, no. 2, pp. 109–113, 1980.

[9] N. S. Singh, A. Jain, and A. Kapoor, "Determination of the solar cell junction ideality factor using special trans function theory (STFT)," *Sol. Energ. Mat. Sol. C.*, vol. 93, no. 8, pp. 1423–1426, 2009.

[10] A. Chatterjee, A. Keyhani, and D. Kapoor, "Identification of photovoltaic source models," *IEEE Trans. Energy Convers.*, vol. 26, no. 3, pp. 883–889, Sep. 2011.

[11] D. Pysch, A. Mette, and S. Glunz, "A review and comparison of different methods to determine the series resistance of solar cells," *Sol. Energ. Mat. Sol. C.*, vol. 91, no. 18, pp. 1698–1706, 2007.

[12] D. Sera and R. Teodorescu, "Robust series resistance estimation for diagnostics of photovoltaic modules," in *35th IEEE IECON*, 2009, pp. 800–805.

[13] G. H. Yordanov, O.-M. Midtgård, and T. O. Saetre, "Series resistance determination and further characterization of c-si PV modules," *Renew. Energ.*, vol. 46, no. 10, pp. 72–80, 2012.
[14] Y. S. Kim, S.-M. Kang, B. Johnston, and R. Winston, "A novel method to extract the series resistances of individual cells in a photovoltaic module," *Sol. Energ. Mat. Sol. C.*, vol. 115, no. 8, pp. 21–28, 2013.
[15] A. Laudani, F. R. Fulginei, and A. Salvini, "Identification of the one-diode model for photovoltaic modules from datasheet values," *Sol. Energy*, vol. 108, pp. 432–446, 2014.
[16] S. Lineykin and A. Kuperman, "Issues in modeling amorphous silicon photovoltaic modules by single-diode equivalent circuit," *IEEE Trans. Ind. Electron.*, vol. 61, no. 99, 2014.
[17] Y. A. Mahmoud, W. Xiao, and H. H. Zeineldin, "A parameterization approach for enhancing PV model accuracy," *IEEE Trans. Ind. Electron.*, vol. 60, no. 12, pp. 5708–5716, 2013.
[18] F. Adamo, F. Attivissimo, A. D. Nisio, and M. Spadavecchia, "Characterization and testing of a tool for photovoltaic panel modeling," *IEEE Trans. Instrum. Meas.*, vol. 60, no. 5, pp. 1613–1622, May 2011.
[19] Y. Mahmoud, W. Xiao, and H. H. Zeineldin, "A simple approach to modeling and simulation of photovoltaic modules," *IEEE Trans. Sustain. Energy*, vol. 3, no. 1, pp. 185–186, Jan. 2012.
[20] S. Lineykin, M. Averbukh, and A. Kuperman, "Five-parameter model of photovoltaic cell based on STC data," in *27th IEEE Conv. Electr. Electron. Eng.*, Eilat, Israel, Nov. 2012, pp. 1–5.
[21] A. Izadian, A. Pourtaherial, and S. Motahari, "Basic model and governing equation of solar cells used in power and control applications," in *IEEE Energy Conv. Congr. Expo.*, Raleigh, NC, Sep. 2012, pp. 1483–1488.
[22] M. Al-Rashidi, M. Al-Hajri, K. El-Naggar, and A. Al-Othman, "A new estimation approach for determining the I-V characteristics of solar cells," *Sol. Energy*, vol. 85, no. 7, pp. 1543–1550, 2011.
[23] H. Qin and J. W. Kimball, "Parameter determination of photovoltaic cells from field testing data using particle swarm optimization," in *IEEE PECI*, no. 1-4, 2011.
[24] J. J. Soon and K.-S. Low, "Optimizing photovoltaic model parameters for simulation," in *IEEE 21st ISIE*, 2012, pp. 1813–1818.
[25] Y. Li, W. Huang, H. Huang, C. Hewitt, Y. Chen, G. Fang, and D. Carroll, "Evaluation of methods to extract parameters from current-voltage characteristics of solar cells," *Sol. Energy*, vol. 90, pp. 51–57, Apr. 2013.
[26] K. F. Teng and P. Wu, "PV module characterization using Q-R decomposition based on the least square method," *IEEE Trans. Ind. Electron.*, vol. 36, no. 1, pp. 71–75, 1989.
[27] H. Park and H. Kim, "PV cell modeling on single-diode equivalent circuit," in *39th IEEE IECON*, 2013, pp. 1845–1849.
[28] J. Appelbaum, A. Chait, and D. Thompson, "Parameter estimation and screening of solar cells," *Prog. Photovolt: Res. Appl.*, vol. 1, no. 2, pp. 93–106, February 1993.
[29] K. Ishaque and Z. Salam, "An improved modeling method to determine the model parameters of photovoltaic (PV) modules using differential evolution (DE)," *Sol. Energy*, vol. 85, pp. 2349–2359, 2011.
[30] M. S. Ismail, M. Moghavvemi, and T. M. I. Mahlia, "Characterization of pv panel and global optimization of its model parameters using genetic algorithm," *Energ. Convers. Manage.*, vol. 73, pp. 10–25, 2013.
[31] W. Xiao, P. R. Dunford, W. G. Palmer, and A. Capel, "Regulation of photovoltaic voltage," *IEEE Trans. Ind. Electron.*, vol. 54, no. 3, pp. 1365–1374, 2007.
[32] M. G. Villalva, J. R. Gazoli, and F. E. R., "Comprehensive approach to modeling and simulation of photovoltaic arrays," *IEEE Trans. Power Electron.*, vol. 24, no. 5, pp. 1198–1208, 2009.
[33] J. J. Soon and K.-S. Low, "Photovoltaic model identification using particle swarm optimization with inverse barrier constraint," *IEEE Trans. Power Electron.*, vol. 27, no. 9, pp. 3975–3983, Sep. 2012.
[34] A. Laudani, F. R. Fulginei, and A. Salvini, "High performing extracton procedure for the one-diode model of a photovoltaic panel from experimental I-V curves by using reduced forms," *Sol. Energy*, vol. 103, pp. 316–326, 2014.
[35] F. Ghani, M. Duke, and J. Carson, "Numerical calculation of series and shunt resistances and diode quality fator of a photovoltaic cell using the Lambert W-function," *Sol. Energy*, vol. 91, pp. 422–431, 2013.
[36] ——, "Numerical calculation of series and shunt resistance of a photovoltaic cell using the Lambert W-function: Experimental evaluation," *Sol. Energy*, vol. 87, pp. 246–253, 2013.
[37] Q.-G. Wang and Y. Zhang, "Robust identification of continuous systems with dead-time from step responses," *Automatica*, vol. 37, no. 3, pp. 377–390, 2001.
[38] M. Hamdy and R. Call, "The effect of the diode ideality factor on the experimental determination of series resistance of solar cells," *Sol. Cells*, vol. 20, no. 2, pp. 119–126, 1987.
[39] M. C. Di Piazza and G. Vitale, *Photovoltaic Sources: Modeling and Emulation*. Springer, 2012.
[40] T. Easwarkhanthan, J. Bottin, I. Bouhouch, and C. Boutrit, "Nonlinear minimization algorithm for determining the solar cell parameters with microcomputers," *Int. J. Solar Energ.*, vol. 4, pp. 1–12, 1986.

Li Hong Idris Lim (M'14) received her B.Eng. and Ph.D. degrees in Electrical Engineering from the National University of Singapore (NUS). She worked at Vestas Technology R&D from 2008 to 2012. Since 2013, she has been working full-time as an Assistant Professor at University of Glasgow. Her research interests include control of wind energy systems, solar forecasting and system identification, and smart grid.

Zhen Ye received his B.Eng. and M.Eng. degrees in electrical engineering from Wuhan University, China, in 2000 and 2003, respectively. In 2008, he got his Ph.D. degree in Electrical Engineering from the National University of Singapore (NUS). After graduation, he worked in the Solar Energy Research Institute of Singapore (SERIS) as a research scientist. Since 2011, he worked in Renewable Energy Corporation (REC) as a principle engineer for the PV module technology. His research interests include PID control, system identification, PV system monitoring, solar power integrity and smart grid.

Jiaying Ye received her Bachelor degree in microelectronics from Sun-Yat-Sen University in Guangzhou, China. After graduation, she worked in Nanyang Technological University in Singapore as a project officer, studying the resistive switching property of thin-film materials. In 2010, she was awarded a PhD scholarship from the NUS Graduate School for Integrative Sciences and Engineering (NGS) and is currently a PhD candidate in NGS and the Solar Energy Research Institute of Singapore (SERIS) at NUS. Her research interest include indoor characterization of PV modules and outdoor performance analysis for PV systems.

Dazhi Yang received the B.Eng. and M.Sc. degrees from Department of Electrical and Computer Engineering, National University of Singapore, Singapore, in 2009 and 2012, respectively, where he is currently working toward his Ph.D. degree. He is employed full-time by the Solar Energy Research Institute, Singapore. His research interests include statistical modeling for solar irradiance, forecasting methodologies, and environmental data mining.

Hui Du received his Diploma in Mechatronics Engineering from Nanyang Polytechnic in 2010. He is currently pursuing Bachelor in Electronics Engineering from National University of Singapore. He is also a full-time employee at Solar Energy Research Institute of Singapore.